Title	Nano-textured self-assembled aligned collagen hydrogels promote directional neurite guidance and overcome inhibition by myelin associated glycoprotein
Author(s)	Abu-Rub, Mohammad T.; Zeugolis, Dimitrios I.; McMahon, Siobhan; Pandit, Abhay
Publication Date	2011-01-11
Publication Information	Mohammad T. Abu-Rub, Kristen L. Billiar, Maarten H. van Es, Andrew Knight, Brian J. Rodriguez, Dimitrios I. Zeugolis, Siobhan McMahon, Anthony J. Windebank and Abhay Pandit (2011) 'Nano-textured self-assembled aligned collagen hydrogels promote directional neurite guidance and overcome inhibition by myelin associated glycoprotein'. Soft Matter, .
Publisher	Royal Society of Chemistry
Link to publisher's version	http://dx.doi.org/10.1039/C0SM01062F
Item record	http://hdl.handle.net/10379/4230

Soft Matter

PAPER

Nano-textured self-assembled aligned collagen hydrogels promote directional neurite guidance and overcome inhibition by myelin associated glycoprotein†

Mohammad T. Abu-Rub,[a] Kristen L. Billiar,[b] Maarten H. van Es,[c] Andrew Knight,[d] Brian J. Rodriguez,[c] Dimitrios I. Zeugolis,[a] Siobhan McMahon,[a] Anthony J. Windebank[d] and Abhay Pandit*[a]

The development of nerve guidance conduits is constantly evolving as the need arises for therapies for spinal cord injury. In addition to providing a path for regrowing axons to reconnect with their appropriate targets, the structural and biochemical cues provided by these conduits should be permissive for directional neurite outgrowth and be protective against inhibition in the vicinity of the injury site. Here, we adapted the use of iso-electric focusing to drive the alignment of supramolecular fibrils into self-assembled collagen hydrogels (∼300 μm diameter), and tested those hydrogels for the ability to direct and enhance the migration of neurites. Structural characterization revealed anisotropic alignment of nanofibrillar aggregates (∼20 nm diameter), arranged in micron-scale bundles (∼1 to 2 μm diameter) similar to the hierarchical size scales observed in native tissues. Neurite outgrowth extended bidirectionally along the axes of aligned hydrogels. Furthermore, it was shown that, as opposed to poly-D-lysine, neurite outgrowth on aligned hydrogels is not inhibited in the presence of myelin-associated glycoprotein ($p > 0.05$). These results highlight for the first time a structural and biochemical role for iso-electrically aligned collagen hydrogels in controlling neuronal growth, and indicate that the short-term signaling associated with these hydrogels can be used in adjunct therapy following injury to the spinal cord.

1 Introduction

Impaired neurological function following spinal cord injury (SCI) is attributed to widespread loss of axonal connections and subsequent lack of neuronal regeneration.[1] The initial response to injury is characterized by "dystrophic endballs" that appear at the ends of lesioned axons and are incapable of growth in the vicinity of an injured environment.[2] Myelin degradation products, such as myelin-associated glycoprotein (MAG), are also released into the injury site,[3] and a number of secondary reactive events ensue leading to glial scar formation.

The role of molecular self-assembly in biological systems, and the knowledge of basic cellular mechanisms governing axon guidance and migration have been invaluable in providing the basis for tissue-engineered strategies for nerve regeneration.[4,5] Given the highly oriented structure of nerve bundles, directional topographic and biochemical cues remain a convincing approach to direct axonal migration, and complement cellular and/or molecular therapeutics aimed at maximizing the regenerative capacity of neurons post-injury. Prototypical constructs employing longitudinally aligned fibers have mainly focused on providing topographic cues. For example, the structure of scaffolds has been shown to impart guidance cues using nano- and micro-fibrous topographies, as is the case with electrospun fibers.[6–8] More recently, biochemical activity was combined with topographic features in the design of biomaterial scaffolds, in the form of neurotrophic or substrate specific activity.[9–13]

A general consensus has emerged that a combinatorial approach incorporating appropriate topographic and biochemical factors is necessary to provide an environment permissive for nerve regeneration. Mimicking the natural extracellular matrix (ECM) in the design of scaffolds satisfies these requirements. For example, type I collagen is a major component of the ECM in the body. It has been identified as a substrate for neuronal growth *in vitro* and has been shown to play a role in neuronal pathfinding and growth cone guidance.[14,15] As a biochemical factor, one mechanism describing the neuronal permissive nature of collagen is integrin related, whereby an up-regulation of the expression of α2 and β1 integrins is seen.[16] Integrins are a large family of heterodimeric transmembrane proteins that mediate cell

[a]*Network of Excellence for Functional Biomaterials (NFB), National University of Ireland, Galway, Ireland. E-mail: abhay.pandit@nuigalway. ie; Fax: +353 91 495585; Tel: +353 91 495833*

[b]*Department of Biomedical Engineering, Worcester Polytechnic Institute, Worcester, MA, USA*

[c]*Conway Institute of Biomolecular and Biomedical Research, University College Dublin, Belfield, Dublin 4, Ireland*

[d]*Department of Neurology, Mayo Clinic College of Medicine, Rochester, MN, 55905, USA*

† Electronic supplementary information (ESI) available: Figure S1: SEM of collagen hydrogels without post processing. Figure S2: TEM of collagen fibrils. Figure S3: Analysis of neurite lengths and redirected migration on aligned collagen hydrogels. See DOI: 10.1039/c0sm01062f

attachment and extension through ECM binding, and were recently shown to mediate (at least partly) neuronal responses to MAG,[17] one of the identified inhibitory components restricting neuronal growth following SCI. Another mechanism is related to the possible structural cues encoded by the 67 nm periodicity specific of collagen fibrils.[18,19] As a biophysical factor, topographic cues could be related to an intrinsic capacity of collagen monomers to self-assemble under the appropriate conditions into oriented fibrillar networks of nano- and micro-fibrils.[20] This fibrillar topography allows for spatial confinement, anisotropy of growth, and likely leads to increases in integrin expression.[21,22]

Access to self-assembled preparations of collagen fibers has therefore gained a lot of interest in nerve regeneration applications. For example, strong magnetic fields were used to induce the alignment of collagen hydrogels, which were shown to improve peripheral nerve regeneration.[23] However, these hydrogels have low surface area to volume ratios, and are therefore unlikely to be of benefit in the spinal cord, where there is a higher neuron density and would benefit from a larger surface area. Another approach used a microfluidic system to create sheets of collagen matrices with an aligned fibrillar structure to promote neurite outgrowth and orientation.[24] Although successfully implemented *in vitro*, these collagen matrices lack a three-dimensional hierarchical structure such as that of collagen fibrils *in vivo*. Electrospinning, although one of the more popular tissue engineering strategies to fabricate nanoscale scaffolds with fibrillar topography, includes the use of high electrical energies which preclude the use of collagen.[25] More recently, iso-electric focusing has been applied to direct the migration and orientation of collagen monomers in an effort to mimic *in vivo* collagen self-assembly.[26]

To this end, it was hypothesized that iso-electrically aligned nanofibrous collagen hydrogels provide necessary topographic and substrate specific cues for directional axon guidance and migration and can overcome myelin-induced inhibition of neurite outgrowth *via* a contact guidance mechanism. The aim of this study was to test whether the structural anisotropy of iso-electrically aligned collagen hydrogels is able to enhance the alignment and direct the migration of neurite extensions from differentiated PC12 cells and dorsal root ganglion (DRG) explants, and whether this effect is related to a self-assembly dependent process. We utilized a neurite outgrowth assay to detect absolute neurite lengths and degree of alignment of neurite extensions on aligned collagen hydrogels. To evaluate the potential use of these aligned collagen hydrogels as adjunct therapy for spinal cord injury, we tested their effect on neurite outgrowth in an inhibitory assay using MAG.

2 Results

2.1 Fabrication of anisotropic fibrous collagen hydrogels and surface characterization

The electrochemical reaction creates a pH gradient in a collagen solution to condense dilute collagen monomers and induce their migration and conformational alignment (Fig. 1A is a schematic of this process). Adjusting the molarity and pH at 37 °C using fiber formation buffer (FFB), referred to as standard buffer treatment, resulted in the formation of a hydrogel with a high

packing density (calculated as 4.3 ± 0.76 mg mL^{-1}). The hydrogel takes the shape of a dense fiber of $\sim$300 μm diameter and $\sim$5 cm length. Using polarized optical microscopy, it was seen that aligned hydrogels contain large birefringent domains along the long axis (Fig. 1E), whereas random hydrogels exhibit random interference colors indicative of random orientation (Fig. 1F). Scanning electron microscopy (SEM) of fixed, dehydrated aligned gels reveals a hierarchical ordering of the newly formed collagen fiber evident in smaller nanofibrils (at 60 000×) with an average diameter of 30 ± 10 nm (Fig. 2A). These fibrils appear to aggregate into micron-level fibrils at 2 μm intervals (Fig. 2B and C) effectively creating microgrooves/ridges running parallel to the axis of aligned fibers. The presence of these micron-level fibrils was also confirmed with atomic force microscopy (AFM) scans over larger areas (up to 50×50 μm; data not shown). In contrast, random collagen hydrogels do not exhibit a hierarchical structure, as evident from the lack of large fibril bundles and a rather uniform nanofibrillar structure (Fig. 2E and F). Collagen fibers not subjected to further buffer treatments after iso-electric focusing (dried fibers) exhibit a nanofibrillar arrangement and larger fibrillar structures similar to that of standard buffer treated fibers (Fig. S1, ESI†).

Similar to what is seen on SEM, TEM examination of 90 nm horizontal cross-sections from aligned fibers reveals nanofibrillar aggregates which appear to adhere to each other, creating larger bundles (Fig. S2A, ESI†). In contrast, a random fibrillar distribution is observed in sections from random hydrogels (Fig. S2B, ESI†). High-resolution AFM scans (5×5 μm) were used to characterize the surface of aligned fibers in order to quantify the nano- and micro-scale topographic features influencing neurite outgrowth and orientation. AFM topographs from aligned fibers reveal that there is a heterogeneous population of nanofibrils with a large number of small fibrils on the order of 20 nm and a smaller number of larger fibrils on the order of 500 nm, the latter exhibiting D-periodicity (Fig. 3).

2.2 Characterization of surface alignment

Anisotropic alignment of the fibrils observed by electron microscopy was assessed using two-dimensional fast Fourier transform (2D FFT) analysis and radial summation (Fig. 4). The degree of alignment in these plots is reported by the height and shape of the peak. A higher, narrower peak in aligned collagen hydrogels corresponds to fibrillar alignment along the long axis (Fig. 4C), whereas the absence of a peak in random hydrogels corresponds to a random fibrillar distribution (Fig. 4D). In contrast to SEM images in the dehydrated state, AFM images reveal no directional bias in the outer fibril layer in the hydrated state, which is likely due to the outer surface during the electrosynthesis process being continuously subject to modification from the addition of collagen monomers.

2.3 Analysis of neuronal behavior and neurite guidance properties

In the current study, fibers from 2.0 mg mL^{-1} collagen solutions were used for neurite outgrowth assays. Embryonic rat DRG explants were cultured on glass substrates layered with strands of aligned hydrogels (fibers) or collagen films as controls. Two
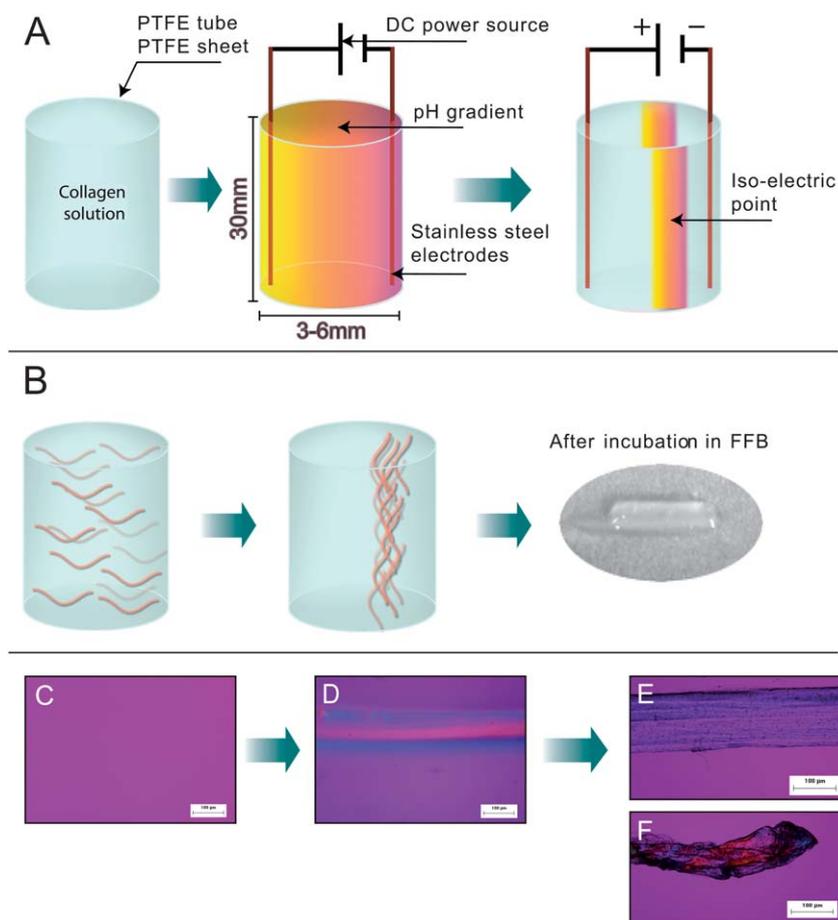
Fig. 1 Iso-electric focusing induces the migration and orientation of collagen monomers. (A) Schematic of the electrochemical process inducing the migration and conformational alignment of collagen monomers. A dialyzed collagen solution (pH 6) was used in conjunction with a hydrophobic surface (PTFE). Stainless steel electrodes connected to a DC power source were immersed into both ends of the collagen solution. Current density of 1.5–3 A m^{-2} and electric field strength of 2 kV m^{-1} were used to generate a pH gradient across the collagen solution and subsequent formation of a collagen band near the cathode at the iso-electric point. (B) Adjusting the molarity and temperature of the newly formed band results in self-assembly and the formation of a collagen hydrogel. (C and D) Polarized optical microscopy images of the collagen solution (C) before and (D) after 30 minutes of electric current application. (E and F) Polarized images of collagen hydrogels after 1 hour incubation with FFB, showing (E) uniform birefringence indicative of uniaxial alignment when iso-electric focusing was used and (F) random interference colors when iso-electric focusing was omitted. Scale bars for C–F are 100 μm.

approaches were used to detect neurite outgrowth behavior. The first was to seed the explants on top of the fibers to evaluate initiation of neurite outgrowth on an anisotropic matrix (Fig. 5), and the second was to seed the explants away from the fibers (on collagen films) and allow the neurites to grow towards the fibers (Fig. S3B, ESI†). The latter assay was evaluated for the ability of topographic cues presented by the aligned fibers to guide neurite extension after growth has initiated. DRG explants seeded on collagen films exhibit no preferential orientation of neurite outgrowth (Fig. 5A). In contrast, DRG explants seeded on top of the aligned fibers show directional outgrowth towards the long axis of the fiber (Fig. 5B). For quantitative assessment of this directional migration, FFT outputs from thresholded images of βIII tubulin stained DRG explants were analyzed. Radial summation of pixel intensities from explants seeded on collagen films results in multiple peaks, indicative of random growth pattern, or starburst appearance (Fig. 5C). In contrast, the single peak generated from FFT outputs of explants seeded on aligned fibers indicates parallel and confined neurite outgrowth

(Fig. 5D). Qualitative evaluation of DRG explants seeded at a distance from the fibers reveals a distinctive growth pattern, whereby groups of neurites change their trajectory to follow that of the axis of underlying fibers. Fig. S3B, ESI† shows initial random outgrowth of neurites, which change trajectory at different points of contact between the neurites and fibers.

2.4 Aligned topography promotes directional polarization

The next step in elucidating the mechanism leading to directional neurite outgrowth was to study the effect of the underlying topography on controlling the direction of polarization of individual neurons. Dissociated PC12 cells were used to study neuronal polarity states at the end of the specified culture period. It was observed that as early as 6 hour *in vitro*, the cells seeded on aligned fibers acquire an elliptical shape, with the leading edges parallel to the direction of underlying fibers (data not shown). This phenomenon might contribute to directional polarization of the leading edges, eventually leading to directional neurite
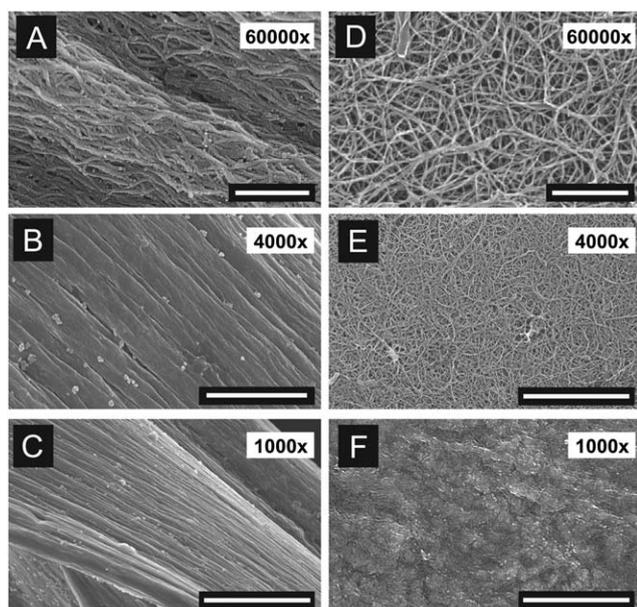
Fig. 2 Self-assembly of aligned collagen fibers. Representative SEM micrographs of collagen structures (A–C) with and (D–F) without iso-electric focusing. (A and D) At a high magnification, the surface of both aligned and random hydrogels is that of nanofibrils. In aligned hydrogels (B and C), these nanofibrils appear to bundle into micron sized fibrils when viewed at a lower magnification. The same bundling is not seen in random hydrogels (E and F) at lower magnifications. Magnifications are labeled at the upper right corner. Scale bars: (A and D) = 500 nm; (B and E) = 10 μm; (C and F) = 25 μm.

outgrowth, and hence an absolute increase in neurite length. Analyzing the length of longest neurite (after 8 days *in vitro* from neurons grown on aligned fibers (bipolar: having two or less neurites per cell body) (Fig. 6A) and neurons grown on random hydrogels (multipolar: having three or more neurites per cell body) (Fig. 6B) shows a significant increase ($p < 0.01$) in the length of longest neurite from neurons on aligned fibers compared to neurons on random hydrogels. However, the sum of lengths of all neurites from neurons on random hydrogels approaches that of the longest neurite from neurons on aligned fibers (Fig. 6C).

At the microstructural level, SEM analysis of differentiated PC12 cells after two days *in vitro* reveals multiple neurites and multiple growth cone filopodial extensions when cells were

seeded on random hydrogels (Fig. 7A and B). In contrast, cells seeded on aligned fibers restrict neurite extensions and growth cone filopodial extensions to the underlying fibrous topography (Fig. 7C and D).

2.5 Collagen self-assembly affects neurite alignment but not neurite length

To examine the role of varying processing parameters on neurite alignment and length, different buffer treatments were tested (K^+ containing for self-fibrillation with D-periodicity, K^+ free to inhibit D-periodicity, and dried to bypass self-fibrillation). These treatments are believed to alter the collagen self-assembly and mechanisms of aggregation and were chosen to elucidate differences in the final composition of structural surfaces affecting cell behavior. Neurite lengths and angles relative to the long hydrogel axis were assessed. The mean angle $\pm$ SD of neurites was $3.7° \pm 19$ ($p > 0.05$) for standard buffer treated hydrogels, $11.8° \pm 33.5$ for dried fibers ($p < 0.05$), $21.3° \pm 22.4$ ($p < 0.05$) for K^+ positive treated hydrogels, and $28.3° \pm 23.7$ ($p < 0.05$) for K^+ free treated hydrogels. There were also no significant differences in neurite lengths between all tested groups (one-way ANOVA, $p > 0.05$). The mean neurite length in μm $\pm$ SEM was 106 ± 7.193 for standard buffer treated hydrogels, 95.93 ± 5.846 for dried fibers, 77.1 ± 3.054 for K^+ positive treated hydrogels, and 80.67 ± 6.504 for K^+ free treated hydrogels.

For characterization of surface stiffness, the different preparations of collagen hydrogels were used as mentioned previously (K^+ positive, K^+ free, and dried). Results from nano-indentation measurements show no difference in Hertzian modulus between different groups of collagen hydrogels (1.35 ± 0.47 kPa, 0.96 ± 0.03 kPa, and 1.12 ± 0.24 kPa for the K^+ positive, K^+ free, and dried, respectively; $p > 0.05$). These levels of stiffness are on the order of soft tissues (*e.g.*, skin) but are orders of magnitude lower than previously measured utilizing similar indentation methods for iso-electrically focused collagen membranes;[27] however in the reported studies the membranes were dried and tested in air rather in a hydrated state which overestimates the stiffness of collagen under physiologic conditions.

### 2.6 Overcoming the inhibitory effect of myelin associated glycoprotein

A soluble Fc chimera of MAG (MAG-Fc) was used as soluble treatment to inhibit neurite outgrowth from neonatal DRG
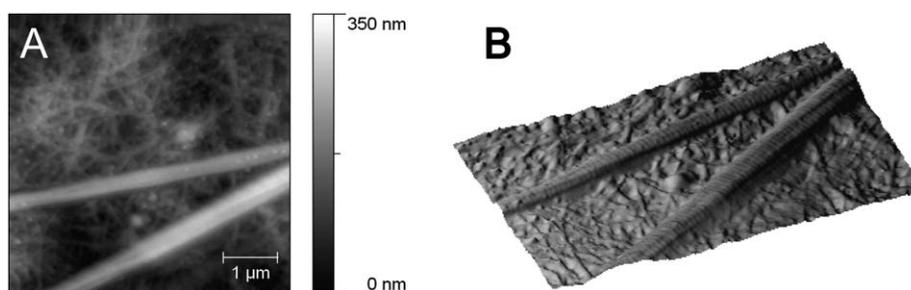

Fig. 3 Structural characterization of aligned collagen fibers. (A) Representative AFM height image of iso-electrically focused collagen fibers. There is a clear heterogeneity of fibrillar structures, showing submicron bundles interspersed with nanofibrils. (B) 3D reconstruction of (A) clearly showing D-periodicity of the submicron fibrils, but not of nanofibrils. Scale bar for A is 100 μm.
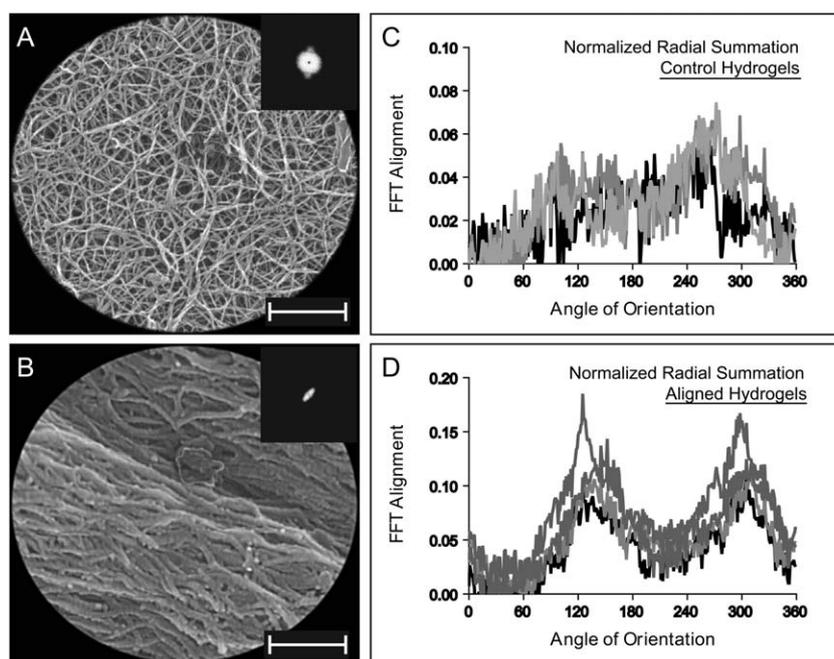
Fig. 4 2D FFT analysis of scaffold anisotropy. (A and B) are high magnification SEM micrographs (60 000×) of random hydrogels and aligned collagen fibers, respectively. The inset in each image is the frequency plot generated by the FFT function of ImageJ. (C and D) are corresponding graphical plots after radial summation of pixel intensities depicting FFT alignment along angles of orientation (0–360°). The random distribution in (C) is indicative of lack of alignment in random hydrogels. In contrast, the high narrow peaks in (D) are indicative of fibrillar alignment. Scale bars for A and B are 350 nm.
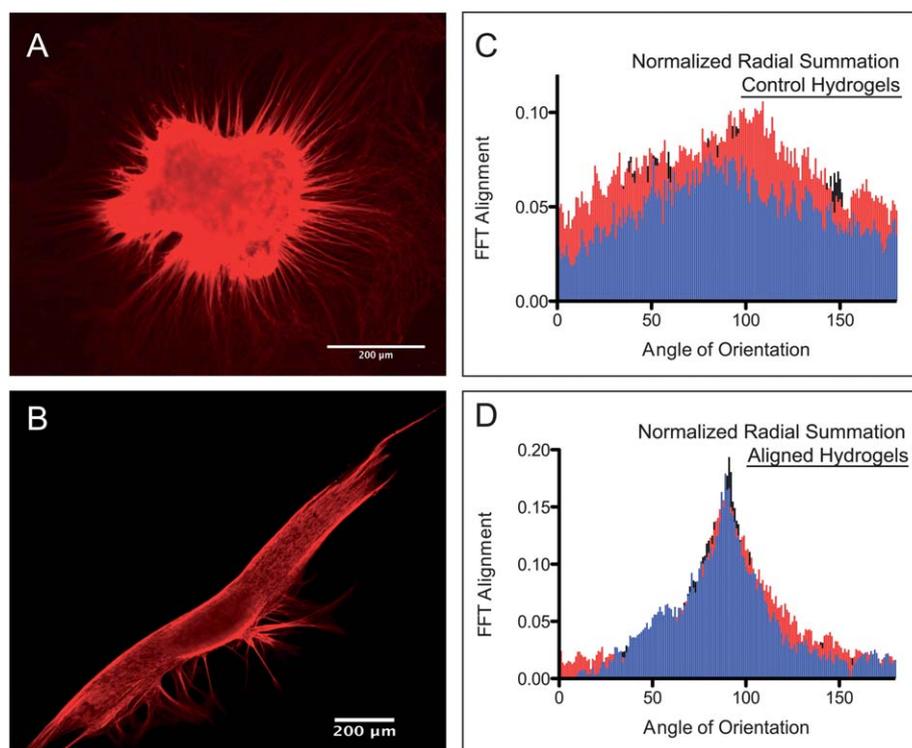
Fig. 5 Aligned collagen fibers confine and promote directional neurite outgrowth. (A) βIII Tubulin stained DRG explant showing random neurite outgrowth (starburst appearance) when seeded on collagen films. (B) Explant seeded on aligned collagen hydrogels extends neurites within the body of the fiber, with parallel neurite outgrowth in both directions. (C and D) are corresponding graphical plots after radial summation of pixel intensities depicting FFT alignment along angles of orientation (0–180°). The random distribution in (C) is indicative of random neurite outgrowth on random hydrogels. The high narrow peak in (D) is indicative of directional neurite outgrowth on aligned hydrogels. Scale bars for A and B are 200 μm.
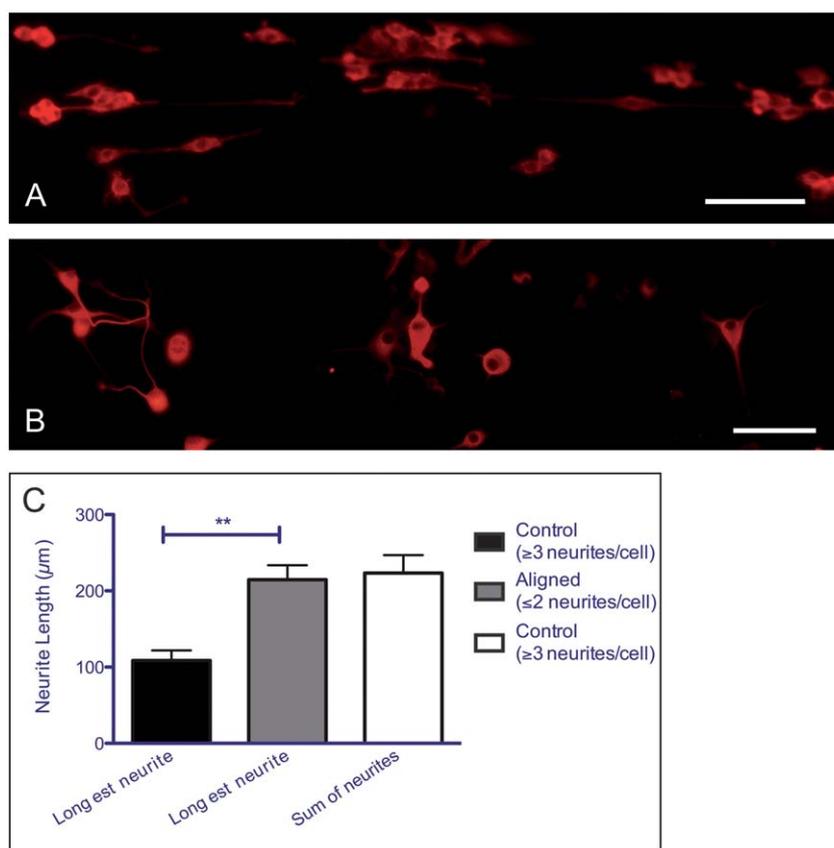
Fig. 6 Aligned fibers direct the polarization and promote absolute neurite outgrowth. (A and B) Representative fluorescent images of tubulin stained PC12 cells with 1 or 2 neurite emanating from cell bodies on aligned fibers (A), and multiple neurites on random hydrogels (B). (C) Summary of neurite lengths from PC12 cells on random collagen hydrogels (leftmost, rightmost bars) and aligned collagen hydrogels (middle bar). There was a significant increase in the length of longest neurite from neurons on aligned fibers (middle bar) compared to neurons on random hydrogels (leftmost bar). The sum of neurite lengths from neurons on random hydrogels (rightmost bar) approximates that of the longest neurite from aligned fibers (middle bar). Scale bars for A and B are 100 μm. Data are the mean ± SEM (**$p < 0.01$).

explants on PDL (Fig. 8A). In contrast, the same effect is not evident when using high-density random collagen hydrogels (3.65 mg mL^{-1}) or aligned collagen hydrogels as substrates (Fig. 8B), indicating that the use of collagen substrates is sufficient to overcome the inhibitory effect associated with the use of MAG. To elucidate a mechanism for a substrate mediated protective effect of collagen against neurite inhibition by MAG, explants on PDL were pretreated with 500 μM MnCl$_2$, a universal activator of integrin receptors, for 60 min before bath application of MAG-Fc. Neurite length measurements reveal no significant difference ($p > 0.05$) between MAG and vehicle treated explants when they were pretreated with Mn^{2+} (Fig. 8A).

3 Discussion

Findings from this study confirm the hypothesis that iso-electrically aligned collagen hydrogels support directional neurite outgrowth and are able to overcome MAG-induced inhibition of neurite outgrowth. We demonstrate with electron and atomic force microscopy that these fibers have a hierarchical structure with ∼30 nm diameter nanofibrils which give rise to D-banded ∼500 nm fibrils and align to form larger bundles of 1–2 μm microfibrils. The result of this bundling is the formation of

micron-scale ridges and grooves on the surface that appear to increase the surface area available for neurite outgrowth and also aid in the alignment of neuronal processes. The surface characterization and studies of neurite outgrowth and migration extend the work of others on iso-electrically focused collagen fibers.[26,28] Further, for the first time on a biomaterial surface, we provide evidence that, in the absence of any surface modification or chemical functionalization, the inhibitory factor and chemo-repellent MAG did not inhibit neurite outgrowth from neonatal DRGs on aligned collagen hydrogels.

3.1 Iso-electric focusing of anisotropic collagen hydrogels

The method for electrochemical fabrication of aligned collagen hydrogels was adapted from previous reports with a few modifications.[26,28] The first modification was the use of hydrophobic surfaces for the electrochemical setup, which was employed to facilitate handling of the formed hydrogels. The second modification involved using a PEG-containing fibrillation buffer to increase the density of the fibrils and trigger collagen self-assembly. PEG is a high molecular polymer that induces volume reduction by water removal, which aids in alignment. When compared to PBS-treated collagen fibers, FFB treated hydrogels
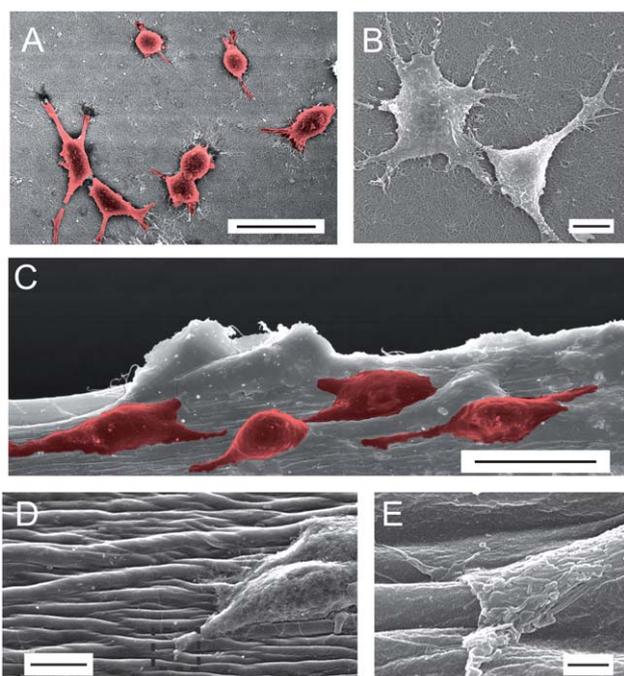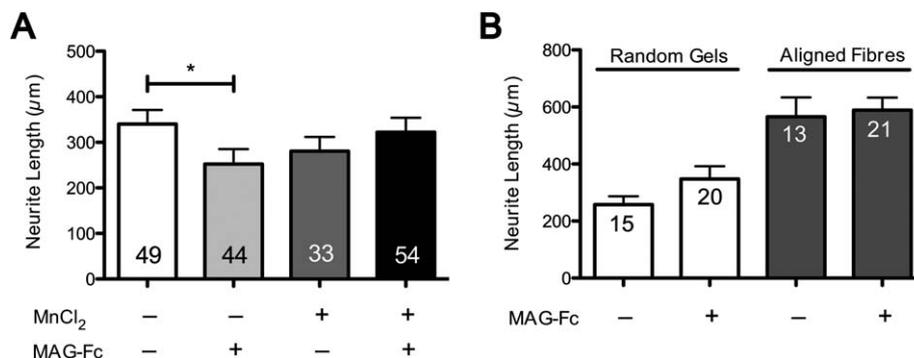
Fig. 7 Anisotropy of substrate directs polarization and reduces filopodial extensions. (A and B) Representative SEM micrographs of PC12 cells (2 days *in vitro*) on random collagen hydrogels showing multipolar neurite outgrowth and multiple filopodial extensions on random nanofibrillar networks. (C–E) Micrographs of PC12 cells on aligned collagen hydrogels showing unipolar neurite outgrowth, and mature lamellipodia on anisotropic fibrillar bundles. In (A and C) the neuronal cell bodies were pseudocolored to highlight neurite extensions. E is a magnified view of the dashed box in D. Scale bars (A and C) = 25 μm, (B and D) = 10 μm, and (E) = 1 μm.

ultimately causes the migration of the monomers in solution until they reach their iso-electric point (pH ≈ 8). This point of high density, and hence low water content, could then initiate lyotropic liquid crystallization, which could explain the highly ordered micron-level fibrillar structures observed even in the absence of further buffer incubations (*i.e.* dried fibers; Fig. S1, ESI†). The resulting structure is similar to the findings from Knight *et al.* of collagen gels prepared by reverse dialysis against PEG, although the nanofibrils on our structure (Fig. S2, ESI†) are larger than the 5 nm fibers found previously.[29] The observation by SEM of moderately aligned nano-sized fibrils (∼30 nm), which bundle together into aligned higher ordered structures (1–2 μm) corroborates previous evidence that collagen electrosynthesis is a multi-step process involving the "localization, organization, and association" of collagen monomers.[28]

3.2 Surface and underlying topography

Since the aim of the present work was to study the functional effect of iso-electrically aligned collagen hydrogels on neurite alignment and outgrowth, we focused a considerable amount of our effort on detailed characterization of the structure, alignment, and properties of the surfaces available for cell growth. The characteristic aligned bands (∼1 to 2 μm in diameter) on SEM (Fig. 2C) have been shown previously for iso-electrically focused collagen fibers.[26] Quantitative analysis utilizing 2D FFT of nano- and micro-fibrils from the SEM micrographs is also in line with previous findings of highly aligned electrospun polymeric scaffolds.[31] In addition, these aligned fibrils have dimensions previously observed to direct cell alignment *in vitro* as discussed below and are also similar to collagen fibrils of endoneurial sheaths surrounding axons *in vivo*.[32] AFM analysis of surface topography shows a network of non-aligned nano-sized fibrils as shown previously for iso-electrically focused thin collagen membranes.[27] In contrast to the previous study, we also show that with our standard buffer treatment the nanofibrils self-assemble into larger D-banded fibrils. Similar to the aforementioned study, to observe these fibrillar structures the surface needed to be slightly dehydrated (ethanol was used previously).[33]

were easier to handle, further streamlining the process and allowing for better reproducibility. The mechanism of fiber formation, and the specific structural features observed, may be explained by a combination of hypotheses from previous reports describing the formation of aligned fibrillar collagen structures.[26,29,30] Collagen molecules acquire different charges as a result of electric current-induced pH gradient formation. This

Fig. 8 Collagen promotes neurite outgrowth after inhibition by soluble MAG-Fc. Summary of mean neurite lengths of neonatal DRG explants (4 days *in vitro*) in μm on PDL (A) or collagen substrates (B), after bath application of MAG-Fc (25 μg mL⁻¹) or MnCl₂ (500 μM) or both (treatment indicated below the graph). (A) There is a significant decrease in neurite length after MAG-Fc treatment on PDL (second from left bar), which is overcome by pretreatment with MnCl₂ (rightmost bar). (B) No effect on neurite length was measured on collagen substrates after addition of MAG-Fc (second from left and rightmost bars). Data are mean ± SEM (n = the number of neurites analyzed per condition; *$p < 0.05$, bracketed comparisons).

3.3 Directional neurite guidance and polarity

Biomaterials have been designed to modulate neuronal behavior, such as growth, migration, and guidance. Recent work has emphasized the role of varying microtopographies on the direction and degree of neurite outgrowth (reviewed in ref. 34). The general consensus is that subcellular-sized (<5 μm) substrate features are supportive for neurite alignment and outgrowth. For example, electrospun fibers of 400–600 nm diameters directed the alignment and migration of DRG neurites.[35] The role of microtopography in specifying neuronal polarity is not very well established, but recent reports point to anisotropy of the substrate as key modulator of neuronal polarity,[36,37] which could be explained by topography-induced microtubule organization.[38,39] In contrast to our results, studies of microtopography do not show evidence of increased neurite lengths when compared to isotropic flat surfaces. Our hypothesis thereof stems from the fact that combined anisotropic features with substrate specific cues provided by collagen are able to both direct and promote neurite outgrowth. Anisotropic collagen structures were fabricated using dip-pen nanolithography, reverse dialysis, dynamic shear flow, magnetic field induced alignment, and more recently iso-electric focusing.[23,26,28,29,40–43] Specifically, aligned collagen constructs were used in neural tissue engineering as nerve guidance conduits.[23,44] Consistent with previous reports of directed neurite elongation along the surface of aligned collagen gels or films, we postulate a similar contact guidance mechanism, and a possible role in specifying neuronal polarity.[45]

In describing the role for nanofibrillar collagen structures, we found that previous reports suggest the presence of an inherent periodicity in the cellular adhesion apparatus, and that cell orientation requires alignment of the cellular apparatus with that of the staggered arrangement of native collagen structures (D-periodicity).[19] Importantly, Poole et al. show that the lack of D-banding in collagen fibrils deposited in a thin film prevents cellular orientation. To further elucidate a correlation between the D-periodicity and neurite alignment, different formulations of collagen hydrogels were made: (1) K⁺ positive for self-fibrillation with D-periodicity; (2) K⁺ free to inhibit D-periodicity; and (3) dried without buffer treatment to bypass self-fibrillation. Analysis of neurite angles relative to the long axes of fibers showed a higher degree of alignment when standard buffer treatment was used compared with the other groups. This difference in alignment is unlikely due to the presence of D-periodicity, as there was no significant difference between K^+ positive and both K^+ free and dried groups. The mechanical properties are likely to be altered due to differences in processing along with the nano-topographic features, and the changes in surface stiffness may contribute to differences in cell response. However, there was no measurable difference in the effective stiffness of surface layers of the aforementioned groups. Differences in alignment are thus likely to be due to the anisotropy in the mechanical properties and structure of the surface rather than the overall surface stiffness (anisotropy cannot be determined by standard nano-indentation).

Taken together, our findings raise important questions as to what structural component of fibrillar collagen translates to a cellular response. Our results lead us to believe that nanofibrillar collagen structures direct the cellular orientation, polarity and eventual neurite outgrowth via a combination of spatial confinement, anisotropy, and a collagen cell–substrate mechanism independent of a staggered arrangement.[46] These mechanisms could lead to integrin clustering near the leading edges of the cell which mature into focal adhesions, and could explain our results related to: (1) directional neuronal polarization and increased neurite length;[47,48] and (2) overcoming response to inhibitory MAG (see Section 3.5).[17]

3.4 Contact mediated axon guidance

The observation that DRG neurites changed their trajectories at different points of contact with the collagen fibers (Fig. S3B, ESI†) is in line with findings from other studies using electrospun poly(ε-caprolactone) (PCL) nanofibers of different topographies and shear flow deposited aligned collagen films.[8,24] One explanation is that the misaligned adhesions do not mature into focal adhesions until facing a favorable topography. This clustering of focal adhesions on the side facing the aligned fibrils results in neurite persistence and aligned neurite outgrowth.[47,49] This finding could benefit in vivo strategies of spinal cord repair, as it would promote directional neurite outgrowth not only from within the scaffold, but also from aberrant growth outside of the scaffold.

3.5 Overcoming response to inhibitory MAG

MAG has been linked to limited axonal regeneration following injury to the adult spinal cord.[50,51] The mechanism with which this inhibition is governed is not fully understood (reviewed in ref. 52). However, several lines of evidence exist for the role of integrins in inhibition of neurite outgrowth in vitro and limited axonal regeneration in vivo (reviewed in ref. 53). ECM proteins, including laminin, fibronectin and collagen, promote neurite outgrowth by recruiting integrin receptors among others. This phenomenon has led to the finding that over-activating or clustering of integrin receptors is involved in overriding the inhibitory effects of MAG.[54] Recent findings associate MAG-induced chemorepulsion with asymmetric redistribution of integrin receptors, a mechanism whereby adhesion to the ECM can become polarized to mediate turning.[17] Here, we identified a role for collagen nanofibers in overcoming inhibition by soluble fragments of MAG. Our inhibitory assay measures neurite outgrowth inhibition in response to bath application of an Fc fragment of MAG. MAG negatively regulates neurite outgrowth on PDL. When tested on collagen substrates, this effect was less evident, and neurite length measurements were not significantly different from their control (vehicle treated) counterparts. These results support previous findings in which laminin and monomeric (non-fibrillar) collagen, through an integrin-dependent mechanism, were shown to override the inhibitory activity of myelin in both substrate-bound and diffusible forms.[54,55] Furthermore, strengthening cell–matrix adhesions by pre-treating cultures with the universal integrin activator, Mn^{2+}, was sufficient to overcome the inhibitory activity of MAG on PDL substrates, a finding in accordance with previous studies where MAG-induced chemorepulsion was abolished after pretreatment with Mn^{2+}, or activation of integrin receptors.[17]

4 Conclusions

In summary, the effect of aligned collagen fibers on the directional orientation, guidance, and outgrowth of neurite processes was studied using iso-electric focusing to induce the migration and conformational alignment of collagen monomers into long ordered and highly aligned fibrils of a hierarchical nature. The iso-electrically aligned hydrogels as substrates proved supportive of unidirectional polarization and neurite outgrowth, even in the absence of post-processing buffer treatments. In addition, evidence was provided to a role for aligned collagen hydrogels in overcoming neurite inhibitory activity by myelin-associated glycoprotein, possibly through a contact guidance mechanism that could be attributed to anisotropy of surface alignment, and/or to a collagen-specific substrate-dependent mechanism. Given the reproducibility, ease of use, and biological relevance of the above approach, these iso-electrically aligned collagen structures appear to be likely candidates for use within nerve guidance conduits for the treatment of spinal cord injury.

5 Experimental

All materials and reagents used in this study were purchased from Sigma Aldrich Ireland Ltd. (Dublin, Ireland) unless otherwise stated. The following type I collagen preparations were used throughout the study: purified porcine dermal atelocollagen (Symatese Biomateriaux, France), and acid soluble rat-tail tendon collagen (BD Biosciences, UK).

5.1 Iso-electric focusing

Dialyzed type-I collagen from two different sources was used as the electrolyte for the electrochemical process. The dialysis ($M_{w\ cut\ off} = 3.5$ kDa) was carried out against acetic acid (20 nM) in ultrapure water (18.2 MΩ cm) at 4 °C for 48 hours to remove salts. Three different concentrations of the collagen solution were tested: 1 mg mL^{-1}, 2 mg mL^{-1}, and 3.7 mg mL^{-1}. The pH of the dialyzed collagen solutions was measured to be in the range of 4.0–6.5. The process of iso-electric focusing of collagen monomers into bands of densely packed collagen fibrils is adapted from a method previously described.[26] Briefly, a hydrophobic surface (PTFE) was used as substrate for the electrochemical cell. Stainless steel electrodes (0.25 mm diameter, Advent, UK) were placed parallel to each other and at varying distances (2, 4, and 6 mm), and the electrodes were connected to a DC voltage power source. The collagen solution (100 μL) was pipetted into the gap between the electrodes (see Fig. 1A for a schematic of this process). The initial voltage supply was set at 3 V, which resulted in a current of ~25 μA and a voltage of ~3 V across the collagen solution as measured by a multimeter. After 30–60 minutes, and visual observation of a dense band near the cathode, the power source was interrupted, and the bundle was lifted carefully with a pair of tweezers. This freshly aligned collagen band was incubated in fiber formation buffer (FFB) made of polyethylene glycol (PEG) (118 mM), $M_w = 8000$ at pH 7.5 and 37 °C for 30 minutes prior to incubation in 1× PBS (0.01 M) overnight.[30] The average diameter of the resulting collagen hydrogel was 0.2–0.4 mm, and was inversely related to the duration of current application.

To determine the effect of processing parameters (*e.g.*, collagen fibrillation conditions and hydration) on cell orientation and collagen band stiffness, other buffer treatments were used instead of FFB and without 1× PBS. These groups include: (1) a K$^+$ containing buffer (200 mM KCl, 50 mM Tris–HCl, pH 7.5); and (2) a K$^+$-free buffer (200 mM NaCl, 50 mM Tris–HCl, pH 7.5). For a further subset of experiments, freshly aligned collagen hydrogels were used immediately after iso-electric focusing without further buffer incubations and allowed to dry at room temperature in semi-humid conditions (referred to as dried fibers).

Air-dried collagen films or randomly oriented collagen hydrogels were used as controls. The method for preparing the latter involved layering a buffer solution (FFB) containing 2 mg mL^{-1} collagen on a PTFE surface, and allowing it to gel at 37 °C for 3 hours in a humid chamber. The hydrogels were further incubated in 1× PBS overnight.

5.2 Polarized optical microscopy

The orientation of the resulting collagen band was monitored and verified by a polarized optical microscope (Olympus BX51, Mason Technologies, Dublin, Ireland), using a first order wavelength gypsum plate (U-TP530) and a polarizer attachment (U-POT).

5.3 Scanning electron microscopy (SEM) and transmission electron microscopy (TEM)

Collagen samples were prepared using a procedure similar to that developed by Raub *et al.* for SEM and TEM imaging of collagen gels.[56] Prior to drying, samples were fixed in 4% para-formaldehyde in 1× PBS for 30 minutes at room temperature and rinsed three times in 1× PBS. For SEM analysis, the samples were post-fixed in 1% osmium tetroxide for 60 minutes at room temperature. The fixed hydrogels were dehydrated in a graded ddH$_2$O/ethanol series: 30%, 50%, 70%, 90%, and two 100% ethanol washes for 10 min each. Following the ddH$_2$O/ethanol washes, the hydrogels were washed with a graded ethanol/hexamethyldisilazane (HMDS) series: 33%, 50%, 66%, and 100% HMDS washes for 15 min each. The dried samples were mounted on SEM sample stages using carbon tape, and sputter coated before analysis with the scanning electron microscope (Hitachi scanning electron microscope S-4700, Hitachi-Hisco Europe GmbH, Berkshire, UK). For TEM analysis, the samples were post-fixed in 2% osmium tetroxide for 1 h, rinsed in cacodylate buffer, dehydrated in graded alcohol (30–100%) and rinsed in propylene oxide. Samples were then infiltrated with agar low viscosity resin (Agar Scientific Ltd., Essex, UK) for 3 days at 60 °C. Sections, 90 nm in thickness, were cut using an ultramicrotome (Leica EM UC6 Ultramicrotome, Leica Microsystems GmbH, Wein, Austria) and stained with uranyl acetate and phosphotungstic acid. Micrographs were captured at magnifications ranging from 30 000× to 100 000× (Hitachi H7500 TEM, Hitachi Scientific Instruments Ltd.).

5.4 Atomic force microscopy (AFM)

To characterize the nanotopography of the collagen hydrogel surfaces in a hydrated state, an Agilent 5500 atomic force

microscope (AFM, Agilent, Palo Alto, CA) equipped with a silicon nitride cantilever (DNP, Veeco) with nominal spring constant of 0.06 N m^{-1} and tip radius ($\sim$20 nm) was utilized in contact mode. The samples were scanned at 1 Hz over a 5 × 5 μm area (512 × 512 pixels). In its fully hydrated state, the nano-fibrous surface being scanned was >100 μm from the glass surface, thus it was extremely deformable and able to move laterally during scanning causing excessive streaking. Thus, to obtain high quality images, samples were stored non-submerged for a minimum of 24 hours at 4 °C in a 100% humidity chamber which partially dehydrated the sample; however, all samples were scanned fully submerged in PBS at room temperature. The periodicity of the banding pattern observed was quantified by image analysis (ImageJ).

The stiffness of the surface of hydrogels treated with K$^+$ and K$^+$-free buffers and the dried hydrogels was determined by microindentation using an Asylum MFP-3D AFM (Asylum Research, Santa Barbara, CA) mounted on an inverted optical microscope Olympus IX71 and equipped with a borosilicate glass sphere-tipped silicon nitride cantilever (Novascan, IO) with a diameter of 5 μm and a nominal spring constant of $\sim$0.06 N m^{-1}. The cantilever spring constant was calibrated using the thermal fluctuation method included in the AFM software. To limit movement of the material, bands were created directly on silanized coverslips. The samples were submerged in their respective buffers (K$^+$ positive and K$^+$ free) and tested at room temperature. Dried collagen bands were rehydrated in PBS for 2 hours. Force–volume mode was used to obtain 36 independent force–indentation curves over a 30 × 30 μm area (*i.e.*, a 6 × 6 sample grid with 5 μm spacing between measurement locations). Indentation limited to 5 nN resulting in an indentation depth of approximately 500 nm; data were taken at 0.5 Hz with a 5 μm withdraw resulting in a rate of 5 μm s^{-1}. Minimal adhesion and hysteresis were observed in the approach and retraction curves (although observed in some locations). The effective Young's modulus at each point was calculated by fitting the approach curves to a Hertz sphere model (assuming a Poisson ratio of 0.2) with the understanding that Hertzian mechanics is only applicable for the linear behavior we observe at small strain. The 36 values were averaged to obtain the best estimate for the given area on the collagen hydrogel. Point-to-point variation in stiffness within a scanning grid was generally 15% (5–30% range), whereas repeated indentation of the same point (36 force–indentation curves) yielded virtually identical stiffness measurements (3% CV). A minimum of three locations on two collagen bands of each type was analyzed.

5.5 PC12 cultures

Rat pheochromocytoma (PC12) cells were obtained from the European Collection of Cell Culture (ECACC). To study neurite growth of PC12 cells on collagen constructs, PC12 cells were seeded at a density of 15 000 cells cm^{-2} for aligned fibers, or mixed with a pre-gelation collagen solution at a density of 15 000 per 100 μL, which was allowed to gel *in situ* at 37 °C as previously described.[57] The cells were grown overnight in full medium [Dulbecco's modified Eagle's medium (DMEM), 10% horse serum, and 5% fetal bovine serum]. From day 2, the medium was replaced with DMEM with 1% horse serum supplement and 50 ng mL^{-1} NGF (2.5 s mouse; Alomone Laboratories, Israel) and replaced every 2 days for 8 days.

5.6 SEM of PC12 cell-seeded collagen scaffolds

PC12 were seeded on collagen scaffolds (gels and fibers) as described above and grown in differentiating medium for 2 days. Following fixation, the samples were prepared for SEM analysis and imaged as described above.

5.7 DRG explants

Embryonic Dorsal Root Ganglia (DRGs) were dissected from E15 rat embryos as previously described.[20] Neonatal DRGs were dissected from P9 rat pups according to procedures described elsewhere.[58] Three DRGs were plated onto each fibrous bundle, or collagen film coated coverslips. The cultures were maintained in complete medium including Neurobasal supplemented with B27, L-glutamine (4 mM; Invitrogen, Ireland), and NGF (10 ng mL^{-1}). The experiments were continued for up to 3 days.

5.8 Immunocytochemistry

The cells were prepared for immunocytochemical analysis by first fixing in 4% paraformaldehyde in 1× PBS for 20 minutes at room temperature. When cells were grown on collagen fibers, the fixative included 0.1% glutaraldehyde and the fixation time was extended to 40 minutes. The fixative was discarded and the samples were washed 3 times with 1× PBS. After permeabilization with 1% Triton-X in 1× PBS, the samples were incubated in blocking buffer (2% BSA, 0.2% Triton-X) for 1 hour. To determine neuronal morphology, a neuronal specific βIII tubulin monoclonal antibody (Tuj1; Abcam, UK) was used at 1 : 500 dilution in blocking buffer. Following overnight incubation in the primary antibody, Alexa Fluor 546 donkey anti-mouse secondary antibody (Invitrogen, Ireland) was used for 1 hour. The samples were mounted using Vectashield mounting medium (Labkem, Ireland), and stored at 4 °C for image analysis. Imaging was done using an upright fluorescent microscope (Olympus BX51, Mason Technologies, Dublin, Ireland), or an inverted epifluorescent microscope (Olympus IX81, Mason Technologies, Dublin, Ireland).

5.9 Analysis of fibril and neurite orientation

2D FFT analysis was chosen as a quantitative measure of alignment of collagen fibrils and subsequent neurite outgrowth. This analysis converts optical information into a frequency distribution. This distribution could then be used to measure pixel intensity across 360°, and indicate the relative distribution of the area of interest along angles of acquisition.[31] For this analysis, uncompressed images (SEM for fibers, and fluorescent images for DRG explants) were used to preserve quality, and were cropped accordingly, despeckled when necessary, and analyzed with the FFT function of ImageJ (v1.42, NIH). The Oval Profile plugin (William O'Connell) was used to calculate radial summation, and the values normalized and plotted as the normalized FFT value *vs.* the angle of acquisition. For analysis of neurite alignment of dissociated PC12 cells, images of fixed, phalloidin stained cells were acquired, and the neurite vertices

traced using the ImageJ plugin NeuronJ.[59] The vectors were then noted, and the slope and angles calculated and plotted in a histogram relative to the long axis of the fibers. For cells seeded on random collagen gels, the angles were calculated relative to an arbitrary axis.

5.10 Analysis of neurite outgrowth

Neurite outgrowth from DRG explants, and differentiated PC12 cells were determined from composite images stained with βIII tubulin. When necessary, images were merged using ImageJ (MosaicJ, Philippe Thévenaz), and individual neurites were traced manually using NeuronJ.

5.11 MAG-Fc neurite inhibitory assay

For MAG-induced neurite inhibitory assay, neonatal DRG cells (P9) were seeded on glass coverslips coated with either PDL (100 μg mL^{-1}), or with random collagen hydrogels or aligned collagen fibers. The cells were left to adhere overnight in full culture medium, and were maintained with medium changes every 2 days. At 3 DIV, MAG-Fc (25 μg mL^{-1}) or vehicle (BSA, 1 mg mL^{-1}) was added to the culture medium, and the cultures were kept overnight. For experiments involving Mn^{2+}, cultures were pretreated with 500 μM MnCl$_2$ before addition of MAG-Fc or vehicle. Following fixation, the cells were stained as above for neuronal specific βIII tubulin, and imaged. The neurite lengths were measured by tracing neurites manually using NeuronJ.

5.12 Statistical analysis

All statistical analyses were performed using Graphpad Prism Version 5.0b (GraphPad Software, Inc.). Data with a normal distribution (D'Agostino and Pearson omnibus normality test) were assessed using a Kruskal–Wallis one-way ANOVA with Dunn's multiple comparisons. Where a normal distribution was not shown, the non-parametric Mann–Whitney U-test was used, comparing experimental groups to the appropriate control.

Acknowledgements

References

1 M. T. Fitch and J. Silver, *Exp. Neurol.*, 2008, **209**, 294–301.
2 S. Ramon y Cajal, *Degeneration and Regeneration of the Nervous System*, Oxford University Press, London, 1928.
3 G. Yiu and Z. He, *Nat. Rev. Neurosci.*, 2006, **7**, 617–627.
4 S. Thuret, L. D. Moon and F. H. Gage, *Nat. Rev. Neurosci.*, 2006, **7**, 628–643.
5 N. N. Madigan, S. McMahon, T. O'Brien, M. J. Yaszemski and A. J. Windebank, *Respir. Physiol. Neurobiol.*, 2009, **169**, 183–199.
6 M. J. Mahoney, R. R. Chen, J. Tan and W. M. Saltzman, *Biomaterials*, 2005, **26**, 771–778.
7 F. Johansson, P. Carlberg, N. Danielsen, L. Montelius and M. Kanje, *Biomaterials*, 2006, **27**, 1251–1258.
8 J. Xie, M. R. MacEwan, X. Li, S. E. Sakiyama-Elbert and Y. Xia, *ACS Nano*, 2009, **3**, 1151–1159.
9 N. Gomez, Y. Lu, S. Chen and C. E. Schmidt, *Biomaterials*, 2007, **28**, 271–284.
10 S. Patel, K. Kurpinski, R. Quigley, H. Gao, B. S. Hsiao, M. M. Poo and S. Li, *Nano Lett.*, 2007, **7**, 2122–2128.
11 S. Y. Chew, R. Mi, A. Hoke and K. W. Leong, *Adv. Funct. Mater.*, 2007, **17**, 1288–1296.
12 V. M. Tysseling-Mattiace, V. Sahni, K. L. Niece, D. Birch, C. Czeisler, M. G. Fehlings, S. I. Stupp and J. A. Kessler, *J. Neurosci.*, 2008, **28**, 3814–3823.
13 A. Mata, L. Hsu, R. Capito, C. Aparicio, K. Henrikson and S. I. Stupp, *Soft Matter*, 2009, **5**, 1228–1236.
14 D. C. Turner, L. A. Flier and S. Carbonetto, *J. Neurosci.*, 1989, **9**, 3287–3296.
15 K. J. Tomaselli, C. H. Damsky and L. F. Reichardt, *J. Cell Biol.*, 1987, **105**, 2347–2358.
16 C. G. Knight, L. F. Morton, A. R. Peachey, D. S. Tuckwell, R. W. Farndale and M. J. Barnes, *J. Biol. Chem.*, 2000, **275**, 35–40.
17 J. H. Hines, M. Abu-Rub and J. R. Henley, *Nat. Neurosci.*, 2010, **13**, 829–837.
18 J. Jokinen, E. Dadu, P. Nykvist, J. Kapyla, D. J. White, J. Ivaska, P. Vehvilainen, H. Reunanen, H. Larjava, L. Hakkinen and J. Heino, *J. Biol. Chem.*, 2004, **279**, 31956–31963.
19 K. Poole, K. Khairy, J. Friedrichs, C. Franz, D. A. Cisneros, J. Howard and D. Mueller, *J. Mol. Biol.*, 2005, **349**, 380–386.
20 D. A. Cisneros, C. Hung, C. M. Franz and D. J. Muller, *J. Struct. Biol.*, 2006, **154**, 232–245.
21 M. M. Stevens and J. H. George, *Science*, 2005, **310**, 1135–1138.
22 B. Bondar, S. Fuchs, A. Motta, C. Migliaresi and C. J. Kirkpatrick, *Biomaterials*, 2008, **29**, 561–572.
23 D. Ceballos, X. Navarro, N. Dubey, G. Wendelschafer-Crabb, W. R. Kennedy and R. T. Tranquillo, *Exp. Neurol.*, 1999, **158**, 290–300.
24 B. Lanfer, A. Hermann, M. Kirsch, U. Freudenberg, U. Reuner, C. Werner and A. Storch, *Tissue Eng., Part A*, 2010, **16**, 1103–1113.
25 D. I. Zeugolis, S. T. Khew, E. S. Yew, A. K. Ekaputra, Y. W. Tong, L. Y. Yung, D. W. Hutmacher, C. Sheppard and M. Raghunath, *Biomaterials*, 2008, **29**, 2293–2305.
26 X. Cheng, U. A. Gurkan, C. J. Dehen, M. P. Tate, H. W. Hillhouse, G. J. Simpson and O. Akkus, *Biomaterials*, 2008, **29**, 3278–3288.
27 M. R. Kumar, E. F. S. Merschrod and K. M. Poduska, *Biomacromolecules*, 2009, **10**, 1970–1975.
28 H. R. Baker, E. F. S. Merschrod and K. M. Poduska, *Langmuir*, 2008, **24**, 2970–2972.
29 D. P. Knight, L. Nash, X. W. Hu, J. Haffegee and M. W. Ho, *J. Biomed. Mater. Res.*, 1998, **41**, 185–191.
30 D. I. Zeugolis, R. G. Paul and G. Attenburrow, *J. Biomed. Mater. Res., Part B*, 2008, **85**, 343–352.
31 C. E. Ayres, B. S. Jha, H. Meredith, J. R. Bowman, G. L. Bowlin, S. C. Henderson and D. G. Simpson, *J. Biomater. Sci., Polym. Ed.*, 2008, **19**, 603–621.
32 H. J. Gamble and R. A. Eames, *J. Anat.*, 1964, **98**, 655–663.
33 M. Kumar, S. Merschrod and K. Poduska, *Biomacromolecules*, 2009, **10**, 1970–1975.
34 D. Hoffman-Kim, J. A. Mitchel and R. V. Bellamkonda, *Annu. Rev. Biomed. Eng.*, 2010, **12**, 203–231.
35 Y. T. Kim, V. K. Haftel, S. Kumar and R. V. Bellamkonda, *Biomaterials*, 2008, **29**, 3117–3127.
36 A. Ferrari, M. Cecchini, R. Degl Innocenti and F. Beltram, *IEEE Trans. Biomed. Eng.*, 2009, **56**, 2692–2696.
37 J. Y. Lee, C. A. Bashur, N. Gomez, A. S. Goldstein and C. E. Schmidt, *J. Biomed. Mater. Res., Part A*, 2010, **92**, 1398–1406.
38 J. V. Small, B. Geiger, I. Kaverina and A. Bershadsky, *Nat. Rev. Mol. Cell Biol.*, 2002, **3**, 957–964.
39 S. Gomis-Ruth, C. J. Wierenga and F. Bradke, *Curr. Biol.*, 2008, **18**, 992–1000.
40 D. L. Wilson, R. Martin, S. Hong, M. Cronin-Golomb, C. A. Mirkin and D. L. Kaplan, *Proc. Natl. Acad. Sci. U. S. A.*, 2001, **98**, 13660–13664.

41 N. Saeidi, E. A. Sander and J. W. Ruberti, *Biomaterials*, 2009, **30**, 6581–6592.
42 N. S. Murthy, *Biopolymers*, 1984, **23**, 1261–1267.
43 C. Guo and L. J. Kaufman, *Biomaterials*, 2007, **28**, 1105–1114.
44 S. Yoshii, S. Ito, M. Shima, A. Taniguchi and M. Akagi, *J. Tissue Eng. Regener. Med.*, 2009, **3**, 19–25.
45 C. C. Hoogenraad and F. Bradke, *Trends Cell Biol.*, 2009, **19**, 669–676.
46 K. K. Parker, A. L. Brock, C. Brangwynne, R. J. Mannix, N. Wang, E. Ostuni, N. A. Geisse, J. C. Adams, G. M. Whitesides and D. E. Ingber, *FASEB J.*, 2002, **16**, 1195–1204.
47 A. Ferrari, M. Cecchini, M. Serresi, P. Faraci, D. Pisignano and F. Beltram, *Biomaterials*, 2010, **31**, 4682–4694.
48 M. L. Condic and P. C. Letourneau, *Nature*, 1997, **389**, 852–856.
49 E. Robles and T. M. Gomez, *Nat. Neurosci.*, 2006, **9**, 1274–1283.
50 G. Mukhopadhyay, P. Doherty, F. S. Walsh, P. R. Crocker and M. T. Filbin, *Neuron*, 1994, **13**, 757–767.
51 M. Schafer, M. Fruttiger, D. Montag, M. Schachner and R. Martini, *Neuron*, 1996, **16**, 1107–1113.
52 R. J. Giger, K. Venkatesh, O. Chivatakarn, S. J. Raiker, L. Robak, T. Hofer, H. Lee and C. Rader, *Restor. Neurol. Neurosci.*, 2008, **26**, 97–115.
53 M. L. Lemons and M. L. Condic, *Exp. Neurol.*, 2008, **209**, 343–352.
54 S. Laforest, J. Milanini, F. Parat, J. Thimonier and M. Lehmann, *Mol. Cell. Neurosci.*, 2005, **30**, 418–428.
55 S. David, P. E. Braun, D. L. Jackson, V. Kottis and L. McKerracher, *J. Neurosci. Res.*, 1995, **42**, 594–602.
56 C. B. Raub, V. Suresh, T. Krasieva, J. Lyubovitsky, J. D. Mih, A. J. Putnam, B. J. Tromberg and S. C. George, *Biophys. J.*, 2007, **92**, 2212–2222.
57 M. R. Parkhurst and W. M. Saltzman, *Biophys. J.*, 1992, **61**, 306–315.
58 A. Hall, *Curr. Protoc. Neurosci.*, 2006.
59 E. Meijering, M. Jacob, J. C. Sarria, P. Steiner, H. Hirling and M. Unser, *Cytometry, Part A*, 2004, **58**, 167–176.